Scalability Analysis of a LoRa Network Under Imperfect Orthogonality

Aamir Mahmood , *Member, IEEE*, Emiliano Sisinni , *Member, IEEE*,
Lakshmikanth Guntupalli , *Member, IEEE*, Raúl Rondón, Syed Ali Hassan , *Senior Member, IEEE*,
and Mikael Gidlund , *Senior Member, IEEE*

Abstract—**Low-power wide-area network (LPWAN) technologies are gaining momentum for Internet-of-things applications since they promise wide coverage to a massive number of battery operated devices using grant-free medium access. LoRaWAN, with its physical (PHY) layer design and regulatory efforts, has emerged as the widely adopted LPWAN solution. By using chirp spread spectrum modulation with qausi-orthogonal spreading factors (SFs), LoRa PHY offers coverage to wide-area applications while supporting high-density of devices. However, thus far its scalability performance has been inadequately modeled and the effect of interference resulting from the imperfect orthogonality of the SFs has not been considered. In this paper, we present an analytical model of a single-cell LoRa system that accounts for the impact of interference among transmissions over the same SF (co-SF) as well as different SFs (inter-SF). By modeling the interference field as Poisson point process under duty cycled ALOHA, we derive the signal-to-interference ratio distributions for several interference conditions. Results show that, for a duty cycle as low as 0.33%, the network performance under co-SF interference alone is considerably optimistic as the inclusion of inter-SF interference unveils a further drop in the success probability and the coverage probability of approximately 10% and 15%, respectively, for 1500 devices in a LoRa channel. Finally, we illustrate how our analysis can characterize the critical device density with respect to cell size for a given reliability target.**

Index Terms—**Interference, Internet-of-things (IoT), low-power wide-area networks (LPWANs), LoRaWAN, stochastic geometry.**

A. Mahmood, L. Guntupalli, R. Rondón, and M. Gidlund are with the Department of Information Systems and Technology, Mid Sweden University, Sundsvall 851 70, Sweden (e-mail: aamir.mahmood@ miun.se; lakshmikanth.guntupalli@miun.se; Raul.Rondon@miun.se; mikael.gidlund@miun.se).

E. Sisinni is with the Department of Information Engineering, University of Brescia, Brescia 25123, Italy (e-mail: emiliano.sisinni@ing.unibs.it).

S. A. Hassan is with the School of Electrical Engineering and Computer Science, National University of Sciences and Technology, Islamabad 44000, Pakistan (e-mail: ali.hassan@seecs.edu.pk).

Color versions of one or more of the figures in this paper are available online at http://ieeexplore.ieee.org.

Digital Object Identifier 10.1109/TII.2018.2864681

I. INTRODUCTION

OVER the past few years, the implementation of Internet-of-things (IoT) in a variety of sectors, including smart home, office, city, and industry, has experienced an exponential growth [1]. In general, IoT applications require the network to be low-cost, low-energy, reliable and, given the increasing number of connected devices, scalable. At the moment, IoT applications are supported by available technologies, such as Zigbee, Bluetooth, and WiFi, for short-range communication; and cellular networks (e.g., 3G, LTE, and 5G) for long-reach scenarios [2], [3].

However, applications that require the energy-efficient performance of short-range technologies but aim at reaching longer distances, prove to be a challenge for cellular systems. To this end, low-power wide-area networks (LPWAN) are recently taking the research spotlight [4]. LPWANs provide long range communication by limiting bit rates, making them a viable alternative for these cases. LoRaWAN is one of such emerging solutions supporting many smart applications [5].

Smart metering, for instance, is one of the potential applications of LoRaWAN [6]. The smart metering enables remote monitoring of resource (electricity, water, gas) consumption, which is becoming necessary both for operators and consumers, e.g., for demand response, dynamic pricing, load monitoring, and forecasting [7], [8]. In urban cities, as the massive number of metering devices are to be connected, the choice of the communication technology depends on the number of supported devices and its scalability [9]. In this respect, LoRaWAN with its scalable—*star-of-stars*—network architecture and simple medium access mechanism offers the required elements to support such applications. In a LoRaWAN cell, the nodes communicate with a gateway via a single-hop LoRa link using grant-free pure ALOHA protocol as medium access mechanism, which allows multiple nodes to uplink event-reports without any handshaking. As ALOHA works without any contention mechanism and is prone to collisions, LoRa—the physical (PHY) layer [10]—offers degrees of freedom in carrier frequency (CF), bandwidth (BW), coding rate (CR), and spreading factors (SFs) to orthogonalize transmissions and, thus, can support high-density deployment of devices. Also, thanks to the chirp spread spectrum (CSS) modulation employed by LoRa, the SFs act as virtual channels for a given CF, BW, and CR. Despite the apparent robustness of LoRaWAN technology, a scalability analysis; *how*

does LoRa scale with device density and cell size while ensuring a certain quality of service, is required to understand its potential for enabling smart applications.

A. Related Works and Motivation

In general, the scalability of a LoRa network can be affected by: first, *co-SF interference*, caused by unruly same channel transmissions using the same SF, that can restrict the scalability in plausible high-density deployments if the signal-to-interference ratio (SIR) of the desired transmission is below a certain threshold, and second, *inter-SF interference*, which stems from the imperfect orthogonality among different SFs and implies that the transmissions from different SFs are not completely immune to the adjacent SFs, thus requiring a certain level of SIR protection. A common assumption in the literature is that the different SFs are completely orthogonal to each other, thus providing complete protection to concurrent transmissions of different SFs [11]. Recently in [12], based on simulations and universal software radio peripheral (USRP)-based implementation, the impact of quasi-orthogonality of the SFs on the link-level performance reveals the opposite, thus invalidating that common notion. Although the required SIR protection is low, it can severely affect the network performance in cases when the interfering terminal is closer to the receiver (a gateway) than the desired terminal, usually referred to as the *near-far* conditions.

Apart from assuming the complete orthogonality among SFs, the LoRa performance modeling and analysis under co-SF interference is also limited. In [6] and [13]–[15], the authors analyzed the LoRa performance only by simulations. On the other hand, there exists a few analytical studies in the literature, for instance, in [14] and [16] pure ALOHA was assumed and the concurrent transmissions were considered to be lost regardless of the SIR level at the receiver. Similarly in [5], LoRa capacity was studied based on the superposition of independent pure ALOHA-based virtual networks corresponding to the available SFs per channel. In [11] and [17], on the contrary, the performance of a LoRa system was analyzed under the capture effect, i.e., the SIR of a desired signal is above an isolation threshold for successful packet reception. However in [11], only the strongest co-SF interferer was modeled using stochastic geometry. While in [17], the model considered the capture effect with each co-SF interferer separately wherein the channel fading was also ignored. Therefore, the system level performance of a LoRa network under the aggregate effect of both the co-SF interference and inter-SF interference is yet to be modeled and investigated.

B. Contributions

In this paper, we investigate the scalability of a LoRa network–a multiannuli single cell system–based on uplink coverage probability under the joint effect of both the co-SF and inter-SF interference. The multiannuli structure is a simple yet logical scheme for allocating SFs based on their respective signal-to-noise ratio (SNR) thresholds. In addition, it helps to realize the near-far conditions and, hence, to analyze the impact of inter-SF interference. We apply the tools from stochastic geometry to model the interference field as a Poisson point process (PPP), and include the medium access and control (MAC) and PHY-layer features and regulatory constraints into the model. Thereon, the key contributions of this paper are summarized as follows.

1) The SIR distributions are derived in the presence of dominant co-SF interferer, cumulative co-SF interference, and inter-SF interference, under a realistic path loss model and channel fading. It is shown how two co-SF interference-based distributions differ; the dominant interferer case, giving an upper bound on success probability, loses its imperviousness to cumulative co-SF interference effects with an increase in device density.

2) Using SIR distributions, the coverage probability is evaluated. It is shown that co-SF interference causes a major coverage loss in interference-limited scenarios. However due to imperfect orthogonality, inter-SF interference exposes the network for further 15% coverage loss for a small number of concurrently transmitting end-devices (EDs).

3) Coverage probability contours are presented, which accentuate the significance of our analytical models for scalability analysis and also can act as a valuable tool for dimensioning the cell size and node density under medium access and reliability constrains.

4) How a strategy to allocate SFs to the devices influences the overall network performance is studied using three different SF allocation schemes.

5) An extension framework for modeling interference in a multicell network is formulated based on the presented single-cell model.

The rest of this paper is organized as follows. Section II introduces the LoRa system. Section III presents the network geometry and, signal and channel models. Section IV finds the SNR-based success probability, whereas Section V develops the SIR distributions under interference. Section VI presents numerical results, analyzes the effect of different SF-allocation schemes, and gives a framework to extend our model to a multicell LoRa network. Finally, Section VII concludes this paper.

II. LORA SYSTEM

As an LPWAN solution, the LoRa system consists of two main components: LoRa—a proprietary PHY layer modulation scheme designed by Semtech Corporation [18], and LoRaWAN—the rest of the protocol stack developed, as an open standard, by LoRa Alliance [19]. Fig. 1 summarizes the LoRaWAN architecture and the protocol stack.

A. LoRaWAN Architecture

A LoRa network provides wireless connectivity analogous to cellular systems but optimized in terms of energy efficiency for IoT-focused applications. The network typically follows a hierarchical or *star-of-stars* architecture, where the EDs are connected via LoRa PHY to one or many gateways. The gateway is then connected to a common network server (NetServer) over standard IP protocol stack. The NetServer is finally connected
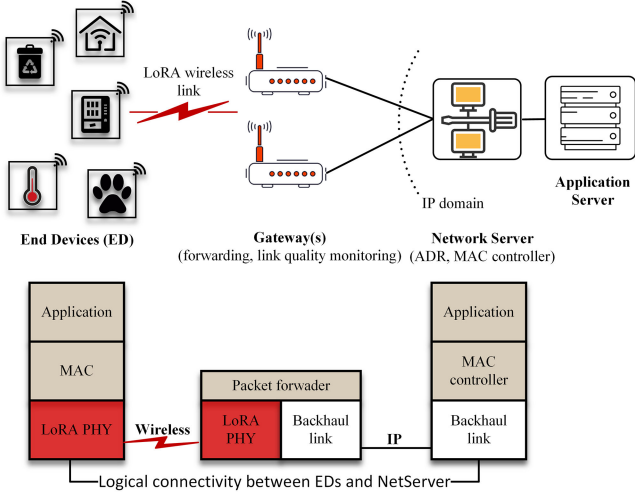
Fig. 1.   Overview of the LoRaWAN architecture.

to an application server (AppServer) over IP. The functionality of each entity is as follows.

1) *ED* supports both the uplink and downlink messages to/from the gateway, generally with a focus on event-triggered uplink transmissions.
2) *Gateway* performs relaying of the messages to EDs or NetServer received over LoRa PHY or IP interface. The gateway is transparent to the EDs, which are logically connected to the NetServer.
3) *NetServer* handles the overall network management, e.g., resource allocation (such as SF and BW) for enabling adaptive data rate, authentication of EDs, etc.
4) *AppServer* is in charge of admitting EDs to the network and taking care of data encryption/decryption.

The LoRa network operates on unlicensed sub-GHz RF bands, which are subject to regulation on medium access duty cycling or listen-before-talk and effective radiated power. The most common approach for the wireless medium access is the simple ALOHA protocol, which is primarily regulated by the NetServer.

B. LoRa PHY Layer

The LoRa PHY—a derivative of CSS modulation—spreads the data symbols with chirps, where each chirp is a linear frequency-modulated sinusoidal pulse of fixed BW $B = f_1 - f_0$ and chirp duration T_c. By varying the chirp duration, quasi-orthogonal signals, acting as virtual channel, can be created. In addition, the chirp duration leads to a tradeoff between the throughput and the robustness against noise and interference. For a fixed T_c, the data symbols are coded by unique instantaneous frequency trajectory, obtained by cyclically shifting a reference chirp. These cyclic shifts, representing symbols, are discretized into multiples of chip-time $T_{\text{chip}} = 1/B$, while only 2^j possible edges in the instantaneous frequency exist. Therefore, each chirp represents j bits where j is referred to as SF. As a result, the modulation signal $m(t)$ of nth LoRa symbol can be

expressed as

$$m(t) = \begin{cases} f_1 + k \cdot (t - nT_{\text{chip}}) & \text{if } 0 \leq t \leq nT_{\text{chip}} \\ f_0 + k \cdot (t - nT_{\text{chip}}) & \text{if } nT_{\text{chip}} < t \leq T \end{cases}$$

where $k = (f_1 - f_0)/T_c$ is the rate of frequency increase over symbol duration T_c.

The NetServer can adapt the data rate by changing the BW $B \in \{125, 250\}$ kHz and SF $\in \{7, \ldots, 12\}$, which together relate to chirp duration as $T_c = 2^{\text{SF}}/B$. Note that the chirp rate remains the same, and equals to B, while the chirp duration (consequently time-on-air) increases drastically with the SF. On the positive side, higher SF yields higher processing gain, and, thus reduces the target SNR for correct reception at the receiver.

Because of ALOHA-based MAC, two or more signals from EDs using the same or different SFs can overlap in time and frequency. In such cases, the demodulator output can be indistinct depending on the isolation threshold and the processing gain of the SFs. The signals using SF $= i$ and SF $= j$ can be decoded correctly only if capture effect [20] occurs, i.e., the SIR of the desired signal is above the isolation threshold. The thresholds for two conditions, co-SF interference $i = j$ and inter-SF interference $i \neq j$, are given by the SIR matrix [12]

$$\mathbf{\Delta}_{\text{[dB]}} = \begin{array}{c} \\ \text{SF}_7 \\ \text{SF}_8 \\ \text{SF}_9 \\ \text{SF}_{10} \\ \text{SF}_{11} \\ \text{SF}_{12} \end{array} \overset{\displaystyle \text{SF}_7 \quad \text{SF}_8 \quad \text{SF}_9 \quad \text{SF}_{10} \quad \text{SF}_{11} \quad \text{SF}_{12}}{\begin{bmatrix} 1 & -8 & -9 & -9 & -9 & -9 \\ -11 & 1 & -11 & -12 & -13 & -13 \\ -15 & -13 & 1 & -13 & -14 & -15 \\ -19 & -18 & -17 & 1 & -17 & -18 \\ -22 & -22 & -21 & -20 & 1 & -20 \\ -25 & -25 & -25 & -24 & -23 & 1 \end{bmatrix}}.$$

(1)

Each element δ_{ij}[dB] in $\mathbf{\Delta}$ is the SIR margin that a packet sent at SF$_i$ must have in order to be decoded correctly if the colliding packet is sent at SF$_j$.

III. SYSTEM, SIGNAL, AND CHANNEL MODELS

A. System Model

We present the uplink system model for a single LoRa gateway, which takes into account the interference from concurrent uplink transmissions on a desired uplink transmission. The notation used in this paper are summarized in Table I. The system model is as follows.

1) EDs are spatially distributed in a deployment region $\mathcal{S} \subseteq \mathbb{R}^2$, which is a two-dimensional (2-D) Euclidean space, according to a homogeneous PPP Φ of intensity (density) $\lambda > 0$, with a gateway located at its origin. The region $\mathcal{S}$ is a disk of radius R and area $A = |\mathcal{S}| = \pi R^2$, and it contains $\Phi(A)$ devices, which is a Poisson random variable with mean $\bar{N} = \lambda A$.
2) Devices make independent decisions to transmit in the uplink using ALOHA. In addition, the devices satisfy the per-frequency band duty cycle constraint of α, as per ETSI specifications [19]. Therefore, the set of all

TABLE I
LIST OF IMPORTANT NOTATIONS

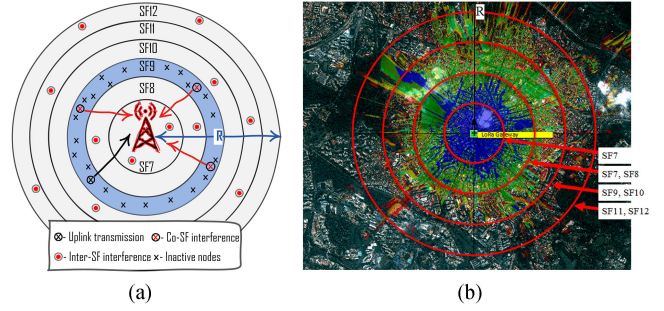| Symbol	Description
$\mathbb{R}^2$	2-dimensional Euclidean space
α	Duty cycle constraint
Φ, Φ_m	PPP of EDs, active EDs with intensity $\lambda, \alpha\lambda$
$K, \mathcal{K}$	Total number of annuli, set of annuli $\{1, \cdots, K\}$
a_i, r_i	Area, width of ith annulus
ℓ_i, ℓ_{i-1}	Outer, inner boundary of ith annulus
v_i	Average number of active EDs in ith annulus
η	Path loss exponent
θ_{SF}	SNR threshold for an SF
δ_{ij}	SIR threshold for successful reception of a packet transmitted at SF_i under a concurrent transmission at SF_j
$h(t), g(t)$	Fading coefficient of the useful, interfering signal
H, G	Channel gain of the useful, interfering signal
$\mathbb{E}[\cdot], \mathbb{P}[\cdot]$	Statistical expectation, probability measure
σ^2	Variance of AWGN noise
N_{SF_x}	Total number of EDs using SF_x
$l(x_i)$	Free space path loss of an ith ED located at x
$\mathbb{1}_i^{\mathrm{SF}_x}$	Indicator function of ith ED using SF_x
P_{SNR}	Success probability in AWGN noise
P_{SIR}^*	Success probability under dominant co-SF interferer
P_{SIR}	Success probability under cumulative co-SF interference
P_{SIR}^{Π}	Success probability under cumulative co-SF & inter-SF interference
$\mathcal{I}_{\mathrm{CSF}}$	Total interference from concurrently active co-SF EDs
$\mathcal{I}_{\mathrm{ISF}}$	Total interference from concurrently active inter-SF EDs
$\mathcal{L}_{\mathcal{I}_{\mathrm{CSF}}}(\cdot)$	Laplace transform of $\mathcal{I}_{\mathrm{CSF}}$
$\mathcal{L}_{\mathcal{I}_{\mathrm{ISF}}}(\cdot)$	Laplace transform of $\mathcal{I}_{\mathrm{ISF}}$
$P_c[\mathcal{Y}]$	Coverage probability with $\mathcal{Y} \in \{P_{\mathrm{SNR}}, P_{\mathrm{SIR}}^*, P_{\mathrm{SIR}}, P_{\mathrm{SIR}}^{\Pi}\}$

Fig. 2. System model. (a) Single gateway LoRa network model with concurrently active nodes in the regions employing same or different SFs. (b) Allocation of SFs under realistic signal propagation conditions. This figure is a modified version of [21] to develop a theoretical model close to the practical deployment of a LoRa network.

transmitting devices at a given time also makes a homogeneous PPP Φ_m of intensity $\alpha\lambda$ due to independent thinning of the PPP.

3) Each device is equipped with an omnidirectional antenna, and transmits at a fixed transmission power p_t in a same channel of BW B.

4) Each device is assigned an SF by the NetServer according to its distance from the gateway. In reality, it can be assigned based on the SNR of the received packets, and the devices in a certain range can use the same SF (see Section VI-C). For simplicity, the network is divided into K disjoint annuli of width $r_i = R/K$ each, starting at the center and moving outward. In this case, if $\mathcal{S}_i$ are disjoint subsets of $\mathcal{S}$, then Φ_m is the superposition of $\Phi_{m,i}$ $(i = 1, \ldots, K)$. The parameter K is determined by the cardinality of the set of available SFs, that is, $K = |\mathrm{SF}|$. The annuli set is denoted as $\mathcal{K} = \{1, \ldots, K\}$, and ith $(1 \leq i \leq K)$ annulus defined by the inner and outer radii ℓ_{i-1} and ℓ_i have the same SF, and the area of the ith annulus is $a_i = \pi r_i^2 (2i - 1)$.

An illustration of a multiannuli single gateway LoRa network with concurrently active nodes in the regions employing same SF as well as different SFs is shown in Fig. 2(a). The simultaneous same SF transmissions interfere at the gateway to a desired transmission, thus resulting in co-SF interference, whereas the inter-SF interference results from concurrent transmissions from all the other regions with devices employing quasi-orthogonal SFs. Note that in realistic signal propagation conditions, the sharp boundaries for SFs allocation as in Fig. 2(a) might not exist. In practice, it is likely to have mixed SNR levels favoring

the allocation of two SFs in the same annulus as in Fig. 2(b). However, our mathematical model can easily address any of such network configurations without loss of generality.

B. Signal and Channel Model

While focusing on a single ED, we investigate its uplink performance under the simultaneous interfering transmissions originating from co-SF and inter-SF regions. Although the inter-SF transmissions are less disruptive (i.e., requiring less SIR threshold), the impact of inter-SF interference must be taken into account for a realistic analysis. Assume that device x_1 located in ith annulus intends to communicate with the gateway, and the devices other than x_1 act as a set of potential interferers. Let $s_1(t, \mathrm{SF}_p)$ be the desired signal transmitted with spreading factor SF_p and experiences block-fading with instantaneous fading coefficient $h(t)$ in addition to power-law path loss. $h(t)$ is a zero-mean circularly symmetric complex Gaussian random variable with unit variance, i.e., $\mathbb{E}[|h|^2] = 1$, which corresponds to Rayleigh fading. Similarly, let $s_i(t, \mathrm{SF}_q)$ be the interfering signal from device i at SF_q over the Rayleigh block-fading channel with fading coefficient $g(t)$. Then, the received signal $r_1(t)$ under co-SF and inter-SF interference can be expressed as

$$r_1(t) = l(x_1)h(t) * s_1(t, \mathrm{SF}_p) + \sum_{j=2}^{N_{\mathrm{SF}_p}} \mathbb{1}_j^{\mathrm{SF}_p} l(x_j) g_j(t) * s_j(t, \mathrm{SF}_p)$$

$$+ \sum_{q \in \mathcal{K} \setminus p} \left(\sum_{k=1}^{N_{\mathrm{SF}_q}} \mathbb{1}_k^{\mathrm{SF}_q} l(x_k) g_k(t) * s_k(t, \mathrm{SF}_q) \right) + n(t).$$

$$(2)$$

In this signal model, other than explaining the notations a few remarks are as follows.

1) $n(t)$ is the additive white Gaussian noise (AWGN) with zero mean and variance $\sigma^2 = N_0 + \mathrm{NF} + 10\log_{10} B$[dBm], where N_0 is the noise power density, NF is the receiver design-dependent noise figure, and B is the channel BW.

2) $\mathbb{1}_i^{\mathrm{SF}_x}$ is an indicator function for a device i transmitting at SF_x, and N_{SF_x} is the total number of devices using SF_x.

3) $l(x_i)$ is the path loss attenuation function, where x_i is the Euclidean distance in meters between the device i and the gateway. From the Friis transmission equation and following a nonsingular model [22], we consider $l(x_i) = \kappa \left[\max (x_i, x_c) \right]^{-\eta}$, where η is the path loss exponent, and $x_c > 0$ is the critical distance to avoid that $l(x_i)$ tends to infinity (i.e., when $x_i \to 0$). In addition, $\kappa = (\lambda_c/4\pi)^2$ where λ_c is the carrier wavelength.

C. Performance Metrics

In absence of any interference, the link performance is determined by an SF specific SNR threshold. On the other hand, when co-SF and/or inter-SF transmissions interfere with the desired signal, the performance can be determined by the SF-dependent SIR. In this respect, the cumulative distribution function (CDF) of SNR/SIR is an important measure for characterizing the link performance; that is, for a given SNR/SIR threshold τ, the CDF gives the link outage probability P_o, whereas the complementary CDF (CCDF) gives the success probability $P_{\mathcal{X}}$, $P_{\mathcal{X}} = 1 - P_o$. If $\mathcal{X} \in \{\text{SNR}, \text{SIR}\}$, then

$$P_{\mathcal{X}} = \mathbb{P}\left[\mathcal{X} \geq \tau\right]. \tag{3}$$

The other important metric, derived from $P_{\mathcal{X}}$, is the coverage probability P_c, which is equivalent to the probability that a randomly chosen device achieves the target SNR/SIR threshold τ. It can be defined as

$$P_c = \mathbb{E}_D\left[\mathbb{P}\left[\mathcal{X} > \tau | D = x_1\right]\right]. \tag{4}$$

In this paper, we analyze the uplink performance of a LoRa network based on the derivations of (3) and (4) for the aforementioned network configuration, while considering the following three interference situations:

1) dominant co-SF interferer—takes into account the interfering power of only the dominant co-SF interfering device;
2) cumulative co-SF interference—considers the impact of cumulative interference from co-SF devices; and
3) cumulative co-SF and inter-SF interference—assumes the joint cumulative interference from co-SF and inter-SF devices.

IV. INTERFERENCE FREE UPLINK PERFORMANCE

When considering an interference-free scenario, uplink outage of the useful signal occurs if SNR of the received signal falls below the threshold θ_{SF}, which depends on the used SF. Let $H := |h|^2$ be the channel gain between the device and the gateway, which is an exponential random variable with unit mean, i.e., $H \sim \exp(1)$. Then, the instantaneous SNR can be defined from (2) as $\text{SNR} = p_t H l(x_1)/\sigma^2$ where p_t is the transmit power of the device. The success probability, as a complement of outage probability, of a device located at distance x_1 from the gateway is given by

$$P_{\text{SNR}}(x_1, \theta_{\text{SF}}) = \mathbb{P}\left[H \geq \frac{\sigma^2 \theta_{\text{SF}}}{p_t l(x_1)}\right] = \exp\left(\frac{\sigma^2 \theta_{\text{SF}}}{p_t l(x_1)}\right). \tag{5}$$

Note that (5) is independent of the device intensities λ and λ_m, and the threshold θ_{SF} remains fixed in an annulus.

V. UPLINK PERFORMANCE ANALYSIS IN POISSON FIELD OF INTERFERERS

In order to analyze the uplink performance in the presence of concurrent transmissions, we utilize stochastic geometry, which is a powerful tool to model stochastic behavior of a network [23]. Stochastic geometry is based on finding the stochastic average of the interference power by summing over the interfering transmissions in the network. To this end, modeling the interference as a shot noise process is widely used (e.g., [23]), considering the noise components as Poisson distributed time instants. For a spatial random process, the time instants are replaced with spatial locations of the nodes while the impulse responses associated to the time instants are replaced with the path loss model.

When the duty cycle constrained devices transmit using the same SF, the concurrently active devices within in annulus are reduced significantly. In this respect, it is interesting to relate the effect of interfering power from the dominant interferer to that of the total interference on the success probability of a desired uplink transmission. The success probability under the dominant interferer can be analyzed based on the extreme order statistics [24].

In what follows, we derive the success probabilities considering the dominant co-SF interferer, which is built upon [11] for the considered path loss model, as well as under the joint impact of cumulative co-SF and inter-SF interference.

A. SIR Success—Dominant Interferer

We consider the success probability of the desired signal under interfering signals of the same SF, however, under the effect of the strongest interferer only. Let us define the strongest interferer k^*, in ith annulus, as

$$k^* = \arg\max_{x_k \in \Phi_{m,i} \setminus x_1} \left\{ \mathbb{1}_k^{\text{SF}_p} p_t G_k l(x_k) \right\} \tag{6}$$

then success probability is determined by the condition that the desired signal is δ times stronger than the dominant interferer

$$P_{\text{SIR}}^*(x_1, \delta) = \mathbb{E}_H\left[\mathbb{P}\left[G_{k^*} l(x_{k^*}) \leq \frac{H l(x_1)}{\delta}\right]\right]. \tag{7}$$

Let $X_{k^*} = G_{k^*} l(x_{k^*})$, then the success probability under the strongest interferer can be calculated from the order statistics. The CDF of the maximum interferer according to the extreme order statistics is $F_{X_{k^*}}(z) = [F_{X_i}(z)]^M$, where M is a Poisson distributed random variable with mean $v_i = \alpha \lambda a_i$, which is the expected number of concurrently transmitting interferers from an annulus of area a_i. If $\mathbb{P}(M = m), m = \{0, 1, 2, \ldots\}$ is the probability mass function of M, then from the total probability theorem, the order statistics in a sample of random size determines $F_{X_{k^*}}(z)$ as

$$F_{X_{k^*}}(x) = \sum_{k=0}^{\infty} \frac{v^k e^{-v}}{k!} [F_{X_i}(x)]^k. \tag{8}$$

By using the series representation $e^x = \sum_{k=0}^{\infty} x^k/k!$, and taking expectation over channel gain H, the success probability from (7) can be determined as

$$P_{\mathrm{SIR}}^*(x_1, \delta) = e^{v_i} \int_0^{\infty} \exp\left(v_i F_{X_i}\left(zl(x_1)/\delta\right)\right) e^{-z} \mathrm{d}z \quad (9)$$

where $F_{X_i}(z)$ is the CDF of product distribution [25] of the probability density function (PDF) of $l(x_i)$ and $G_i \sim \exp(1)$. The distance distribution of the devices to the gateway in ith annulus with boundaries $[\ell_{i-1}, \ell_i)$ and area a_i is $2\pi x/a_i$. Thus, for the considered path loss model, the PDF of $l(x_i)$ is $f_{l(x_i)}(x) = 2\pi\kappa^{\frac{2}{\eta}} x^{-\frac{\eta+2}{\eta}}/(\eta a_i)$ defined over $l(\ell_i) \le x \le l(\ell_{i-1})$, and $F_{X_i}(z)$ is

$$F_{X_i}(z) = \frac{\pi\kappa^{\frac{2}{\eta}}}{a_i}\left[\frac{e^{\frac{-z}{l(x)}}-1}{l(x)^{\frac{2}{\eta}}} - z^{-\frac{2}{\eta}}\Gamma\left(1+\frac{2}{\eta},\frac{z}{l(x)}\right)\right]_{x=\ell_i}^{x=\ell_{i-1}} \quad (10)$$

where $\Gamma(\cdot,\cdot)$ is the upper incomplete gamma function [26].

B. SIR Success—Cumulative Interference

In this section, we perform the SIR-based outage or success probability analysis of the desired signal subjected to aggregate co- and inter-SF interference. The objective is to find how cumulative interference, as apposed to the dominant interferer, affects the link performance considering the dominant interferer analysis to be an upper bound on the outage.

1) SIR Success Under Co-SF Interference: The SIR experienced by the desired signal, from the ith annulus, at the gateway under concurrent co-SF interference is

$$\mathrm{SIR}_{\mathrm{CSF}} = \frac{Hl(x_1)}{\underbrace{\sum_{x_k \in \Phi_{m,i}\backslash x_1} \mathbb{1}_k^{\mathrm{SF}_p} G_k l(x_k)}_{\mathcal{I}_{\mathrm{CSF}}}}. \quad (11)$$

Let $\delta_{ii}[\mathrm{dB}]$ be the threshold needed for the desired signal at SF_i against interferers using the same SF_i, then the condition for success probability $\mathbb{P}\left[\mathrm{SIR}_{\mathrm{CSF}} \ge \delta_{ii}\right]$ can be expanded as

$$\begin{aligned} P_{\mathrm{SIR}}(x_1, \delta_{ii}) &= \mathbb{E}_{\mathcal{I}_{\mathrm{CSF}}}\left[\mathbb{P}\left[H \ge \frac{\delta_{ii}\mathcal{I}_{\mathrm{CSF}}}{p_t l(x_1)}\right]\right] \\ &\stackrel{(a)}{=} \mathbb{E}_{\mathcal{I}_{\mathrm{CSF}}}\left[\exp\left(-\frac{\delta_{ii}\mathcal{I}_{\mathrm{CSF}}}{p_t l(x_1)}\right)\right] \\ &\stackrel{(b)}{=} \mathcal{L}_{\mathcal{I}_{\mathrm{CSF}}}\left(\frac{\delta_{ii}}{p_t l(x_1)}\right) \end{aligned} \quad (12)$$

where (a) in (12) follows from $H \sim \exp(1)$. Also in (b), $\mathcal{L}_{\mathcal{I}_{\mathrm{CSF}}}(\cdot)$ is the Laplace transform (LT) at $s = \delta_{ii}/(p_t l(x_1))$ of the cumulative interference power $\mathcal{I}_{\mathrm{CSF}}$, which can be evaluated with the probability generating functionals (PGFLs). Using the LT

definition, from (11) and (12) we have

$$\begin{aligned} \mathcal{L}_{\mathcal{I}_{\mathrm{CSF}}}(s) &= \mathbb{E}\left[\exp\left(-s\mathcal{I}_{\mathrm{CSF}}\right)\right] \\ &= \mathbb{E}_{\Phi_{m,i},G_k}\left[\exp\left(-s\sum_{x_k \in \Phi_{m,i}\backslash x_1} p_t G_k l(x_k)\right)\right] \\ &= \mathbb{E}_{\Phi_{m,i},G_k}\left[\prod_{x_k \in \Phi_{m,i}\backslash x_1} \exp\left(-sp_t G_k l(x_k)\right)\right] \end{aligned} \quad (13)$$

where the expectation is over the point process $\Phi_{m,i}$ and channel gain G. The expectation with respect to G can be moved inside, as G is independent from the PPP. Then, using the moment generation function of exponential random variable with $G \sim \exp(1)$ in (13) yields

$$\mathcal{L}_{\mathcal{I}_{\mathrm{CSF}}}(s) = \mathbb{E}_{\Phi_{m,i}}\left[\prod_{x_k \in \Phi_{m,i}\backslash x_1} \frac{1}{1+sp_t l(x_k)}\right]. \quad (14)$$

By using the PGFL of homogeneous PPP [23] with respect to the inner function of (14), i.e., $\mathbb{E}\left[\prod_i \mathcal{U}(x_i)\right] = \exp\left(-\lambda \int_{\mathbb{R}^2} 1 - \mathcal{U}(x)dx\right)$ for any no-negative function $\mathcal{U}(x_i)$, we have

$$\mathcal{L}_{\mathcal{I}_{\mathrm{CSF}}}(s) = \exp\left(-\alpha\lambda \int_{\mathbb{R}^2}\left(1 - \frac{1}{1+sp_t l(x_j)}\right)\mathrm{d}x\right). \quad (15)$$

Finally, the transformation of Cartesian to polar coordinates $x_j = (x, \theta)$ gives

$$\mathcal{L}_{I_{\mathrm{CSF}}}(s) = \exp\left(-2\pi\alpha\lambda \int_{\ell_{i-1}}^{\ell_i^-} \frac{sp_t l(x)}{1+sp_t l(x)} x\mathrm{d}x\right) \quad (16)$$

where ℓ_{i-1} and ℓ_i^- are the inner and outer boundaries of the ith annulus. Replacing s gives the success probability of a zero-noise network, i.e., for an interference-limited case.

Using (16) in (13), we get the success probability of a packet from a device located at distance x_1, within an annulus $[\ell_{i-1}, \ell_i)$, from the gateway under same SF interference as

$$P_{\mathrm{SIR}}(x_1, \delta_{ii}) = \exp\left(-2\pi\alpha\lambda\mathcal{I}\left(x_1, \delta_{ii}, \{\ell_{i-1}, \ell_i\}\right)\right) \quad (17)$$

where

$$\mathcal{I}\left(x_1, \delta_{ii}, \{\ell_{i-1}, \ell_i\}\right) = \int_{\ell_{i-1}}^{\ell_i^-} \frac{\delta_{ii}l(x)}{l(x_1)+\delta_{ii}l(x)} x\mathrm{d}x. \quad (18)$$

2) SIR Success Under Inter-SF Interference: When inter-SF interference is considered, the outage occurs when the SIR of the desired signal of SF_i goes below the threshold $\delta_{ij}[\mathrm{dB}]$ [see SIR matrix (1)] when the concurrent transmissions of quasi-orthogonal SFs SF_j are interfering. Let the device transmitting the useful signal be located in the ith annulus, then concurrent transmissions with orthogonal SFs will originate from $\mathcal{K}\backslash i$ annuli, i.e., all annuli except ith annulus, and SIR can be defined

as

$$\text{SIR}_{\text{ISF}} = \frac{Hl(x_1)}{\underbrace{\sum_{j=1,j\neq i}^{K} \sum_{x_k \in \Phi_{m,j}} \mathbb{1}_k^{\text{SF}_q} G_k l(x_k)}_{\mathcal{I}_{\text{ISF}}}}. \quad (19)$$

However, the desired signal has a different SIR margin with respect to the interfering transmissions from each annulus. As all annuli are disjoint, from the independence of PPP, the success probability of the desired transmission in the ith annulus under inter-SF interference, originating from $\mathcal{K}\backslash i$ annuli, can be determined from (12) as

$$P_{\text{SIR}}(x_1, \delta_{ij}) = \prod_{j=1,j\neq i}^{K} \mathcal{L}_{\mathcal{I}_{\text{ISF}}}\left(\frac{\delta_{ij}}{p_t l(x_1)}\right) \quad (20)$$

where $\mathcal{L}_{\mathcal{I}_{\text{ISF}}}(\cdot)$ is the LT of cumulative inter-SF interference power at $s = \delta_{ij}/(p_t l(x_1))$, which can be found from (13)–(16)

$$P_{\text{SIR}}(x_1, \delta_{ij}) = \exp\left(-2\pi\alpha\lambda \sum_{j=1,j\neq i}^{K} \mathcal{I}\left(x_1, \delta_{ij}, \{\ell_{j-1}, \ell_j\}\right)\right) \quad (21)$$

where $\mathcal{I}(\cdot)$ is defined in (18).

3) SIR Outage Under Co- and Inter-SF Interference: For a device located at x_1 in the ith annulus, the success probability under co- and inter-SF interference together can be determined from (17) and (21) as

$$P_{\text{SIR}}^{\text{II}}(x_1, \delta_{ij}) = \exp\left(-2\pi\alpha\lambda \sum_{j=1}^{K} \mathcal{I}\left(x_1, \delta_{ij}, \{\ell_{j-1}, \ell_j\}\right)\right). \quad (22)$$

C. Coverage Analysis

Based on the analyzed success probabilities, $\mathcal{Y} \in \{P_{\text{SNR}}, P_{\text{SIR}}^*, P_{\text{SIR}}, P_{\text{SIR}}^{\text{II}}\}$, the coverage probability can be determined from (4) by averaging over the distance distribution of x_1, $f_D(x_1)$ as

$$P_c[\mathcal{Y}] = \int_{d>0}^{R} \mathcal{Y} \cdot f_D(x_1)\mathrm{d}x_1. \quad (23)$$

Using the PDF of the distance of a uniformly distributed random devices within the area πR^2, the coverage probability for the assumed geometry of the LoRa network, from (23), is

$$P_c[\mathcal{Y}] = \frac{2}{R^2} \sum_{i=1}^{n} \left(\int_{\ell_{i-1}}^{\ell_i^-} \mathcal{Y} \cdot x_1 \mathrm{d}x_1\right). \quad (24)$$

VI. RESULTS AND DISCUSSION

In this section, we validate the analytical models for success probability and network coverage through Monte Carlo simulations. In the simulation setup, the devices are distributed in a disk of radius R according to a homogeneous PPP of intensity $\lambda = \bar{N}/A$, where $\bar{N}$ is the average number of devices. The disk is divided into K disjoint annuli of equal width R/K (unless specified otherwise), where K is the number of available SFs.

TABLE III
LORA SF SPECIFIC CHARACTERISTICS

Annulus	SF	SNR thresh. (θ) (dB)	Range (m)
1	7	−6	$\ell_0 - \ell_1$
2	8	−9	$\ell_1 - \ell_2$
3	9	−12	$\ell_2 - \ell_3$
4	10	−15	$\ell_3 - \ell_4$
5	11	−17.5	$\ell_4 - \ell_5$
6	12	−20	$\ell_5 - R$

To calculate the success probability of a desired uplink transmission at the gateway, we move the node location from the inner to the outer radius of an annulus with a minimal fixed step size. At each location, the success of the desired transmission is evaluated for two conditions: first, the SNR of the useful signal is above the SF-dependent SNR threshold, second, the SIR of the same signal exceeds the SIR threshold under simultaneously active devices causing co-SF and inter-SF interference. The set of concurrently transmitting devices is determined by the duty cycle parameter α. Then, we find the success probability at each distance as expected frequency over 10^5 independent realizations of nodes' distribution. Similarly, we find the coverage probability with respect to $\bar{N}$ under noise and the considered interference conditions.

The matching of the numerical and simulation results demonstrates the accuracy of the developed models. The parameters used to obtain the results are given in Table II while the allocation of SFs in a single-cell multiannuli network is based on Table III, where the SF-dependent SNR thresholds are from [10]. The SIR thresholds are given in SIR matrix (1).

A. Success Probability

In Fig. 3, the success probability of the assumed LoRa network for the studied SNR- and SIR-based conditions is shown for two different cell sizes; $R = 6$ km in Fig. 3(a) and $R = 12$ km in Fig. 3(b). The P_{SNR} curve from (5) shows that the success probability decreases with respect to the distance from the gateway due to path loss and fading. It is, however, interesting to note how success probability improves at the annuli transitions (e.g., at $x_1 \in \{1, 2, \ldots, 5\}$ km for $R = 6$ km)
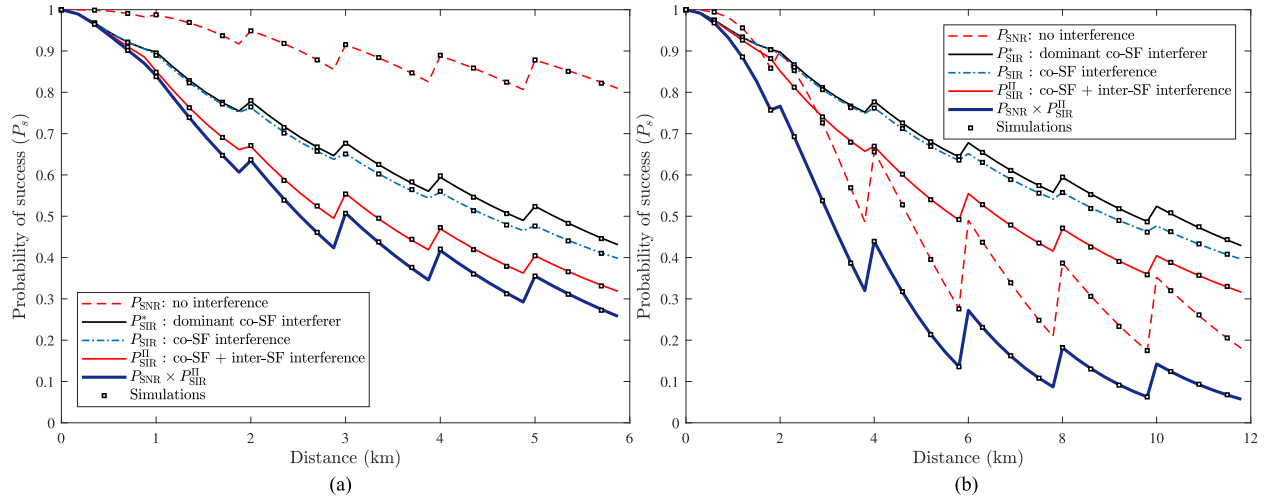
Fig. 3.   Outage probability under studied outage conditions with average number of EDs $\bar{N} = 1500$, and $\eta = 3$. Solid lines are obtained via numerical evaluation of (9), (17), and (22), whereas the markers '□' represent simulation results. (a) $R = 6$ km. (b) $R = 12$ km.

with the use of higher SFs. The gain in the performance is due to the lower receiver sensitivities, and hence, the lower required SNRs for higher SFs. As a result, a higher SF yields a positive performance jump at the inner boundary of each annulus and the multiannuli allocation of SFs gives a saw-tooth trend to the interference-free success probability. Note that the gain depends on the SF-dependent SNR threshold θ_{SF} and on the strategy to allocate SFs. In these results, we assume an equal-interval-based (EIB) annuli structure, as described in Section III-A, where the EDs in the inner most annulus use the lowest SF and the SFs' strength increases for the outer annuli.

When it comes to study the network performance under self-interference, we use three SIR based metrics: strongest co-SF interferer (P_{SIR}^*), aggregate co-SF interference (P_{SIR}), and aggregate co-SF and inter-SF interference (P_{SIR}^{II}). The respective curves obtained from (9), (16), and (21) are shown in Fig. 3. From these results, we can make the following remarks.

1) In general, the saw-tooth trend in the success probability curves, produced by the ED switching to a higher SF region, is observed in all the considered interference conditions, although less prominent compared to non-interference case. This small gain can be attributed to the relative location of the ED at the inner boundary of the annulus compared to the co-SF interfering EDs, thus making it more probable for the ED to achieve an SIR of at least 1 dB. Despite the small gain, the success probability decreases with the distance from the gateway due to increase in number of EDs causing co-SF and/or inter-SF interference.

2) At annuli boundaries, the small gain in P_{SIR}^*, P_{SIR}, and P_{SIR}^{II} is determined by the co-SF and/or inter-SF-based SIR thresholds in addition to the SF allocation strategy.

3) The success probability under cumulative co-SF interference (P_{SIR}), modeled as a shot-noise process, follows the success probability obtained under dominant interferer (P_{SIR}^*). In fact, P_{SIR}^* serves as an upper bound but it loses its tightness for higher SFs annuli because the number

of EDs is proportional to the area a_i of an annulus, and hence, the impact of cumulative interference increases.

4) The inter-SF interference can cause up to 15% loss in the success probability (P_{SIR}^{II}) as compared to co-SF interference only, which is significant enough to be taken into consideration in a realistic scalability analysis.

The SNR- and SIR-based performance indicators must be observed together to understand the dominant cause of the performance degradation. Although in very dense deployment scenarios, the interference can be a main cause of drop in the performance. However, considering the cell size, limited transmit power of EDs and signal propagation conditions, the impact of background noise must also be accounted for. As can be observed from Fig. 3, the impact of interference on the success probability dominates for a cell of radius $R = 6$ km [see Fig. 3(a)] while for $R = 12$ km, the impact of noise is more than the interference [see Fig. 3(b)]. In essence, as $\bar{N}$ is the same for both cell sizes, we observe that the relative impact of the interference on the desired transmission remains the same. However, the success probability under noise is degraded more in Fig. 3(b) due to a bigger cell size. The overall impact can be deduced based on the joint success probability by multiplying P_{SNR} with P_{SIR}^{II}.

B. Coverage Probability

We also evaluate the network coverage probability $P_c[\mathcal{Y}]$ under the studied success probabilities, i.e., $\mathcal{Y} = \{P_{SNR}, P_{SIR}^*, P_{SIR}, P_{SIR}^{II}\}$ using (24), which is shown in Fig. 4. These results depict the scalability of a LoRa network with an increasing number of EDs for two cell size; $R = 6$ km in Fig. 4(a) and $R = 12$ km in Fig. 4(b). The coverage results can give important guidelines for network dimensioning.

Fig. 4, any subplot, shows that the SNR-based coverage probability ($P_c[P_{SNR}]$) is constant as it is independent of the number of EDs. In essence, it gives the noise-only coverage characteristics with respect to cell size. On the other hand, SIR-based coverage probabilities, i.e., $P_c[P_{SIR}^*]$, $P_c[P_{SIR}]$, and $P_c[P_{SIR}^{II}]$,
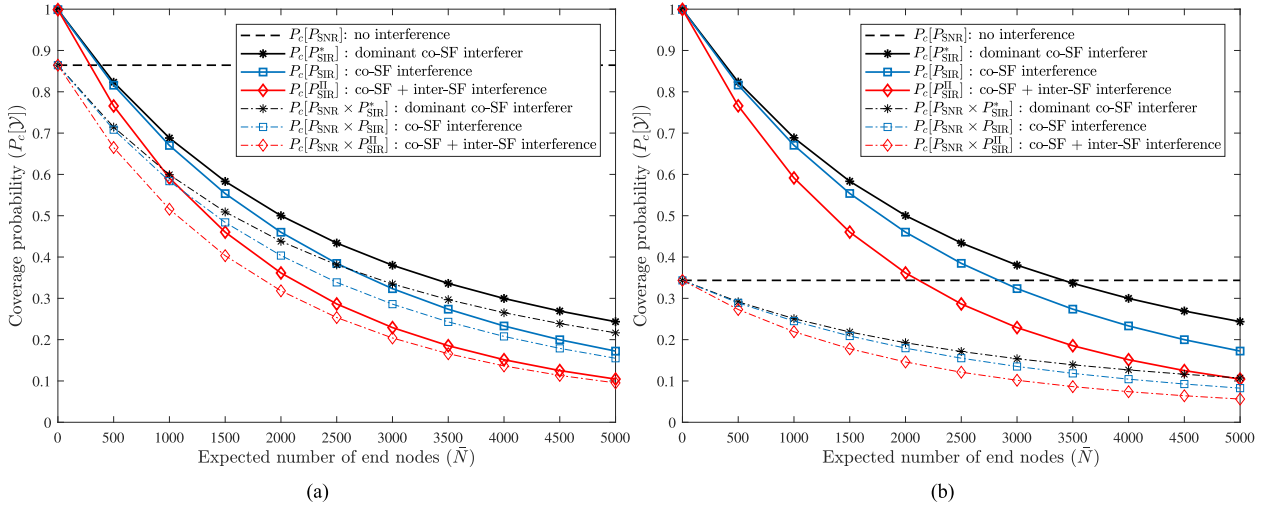
Fig. 4.   Coverage probability with respect to average number of EDs for the studied outage conditions at $\eta = 3$ and two different cell sizes. (a) $R = 6$ km. (b) $R = 12$ km.
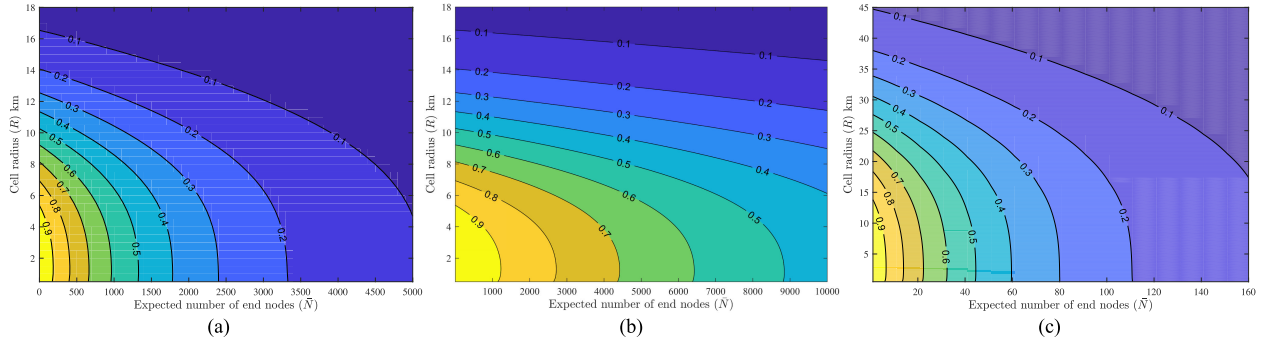

Fig. 5.   Contours of joint coverage probability $P_c\left[P_{\mathrm{SNR}} \cdot P_{\mathrm{SIR}}^{\mathrm{II}}\right]$ for different duty cycle and transmit power configurations at $\eta = 3$. (a) h1.4: EU 868.0–868.6 MHz with three 125 kHz wide channels and the band has 1% duty cycle limitation. ($\alpha = 0.33\%$, $p_t = 14$ dBm.) (b) h1.5: EU 868.7–869.2 MHz offers two channels of 125 kHz BW each, and duty cycle limitation on the band is 0.1%. ($\alpha = 0.05\%$, $p_t = 14$ dBm.) (c) h1.6: EU 869.4–869.65 MHz has one 125 kHz channel, and duty cycle cannot exceed 10%. ($\alpha = 10\%$, $p_t = 27$ dBm.)

decrease exponentially with the increase in EDs. This diminishing performance is the direct result of the increasing co-SF and inter-SF interference, which together make it less likely for the desired signal to achieve the desired SIR protection. From any of these subfigures, it can be observed that the coverage probability under dominant co-SF interferer only ($P_c[P_{\mathrm{SIR}}^*]$) is optimistic compared to the one given by aggregate co-SF interference ($P_c[P_{\mathrm{SIR}}]$). $P_c[P_{\mathrm{SIR}}^*]$ gives an upper bound on co-SF interference and it reduces its tightness with the increase in the device density. In comparison to $P_c[P_{\mathrm{SIR}}]$, the coverage probability under both the co-SF and inter-SF ($P_c[P_{\mathrm{SIR}}^{\mathrm{II}}]$) has a larger decay constant. As a result, $P_c[P_{\mathrm{SIR}}^{\mathrm{II}}]$ decreases much faster with respect to the number of EDs, and the imperfect orthogonality together with same SF interference can have up to 15% lower coverage probability than the same SF case only for 1500 devices per LoRa channel.

The impact of cell size on the coverage probability can be observed from Fig. 4(a) and (b). The coverage probability under noise $P_c[P_{\mathrm{SNR}}]$, although independent of device density, changes proportionally to the cell size. Whereas, the SIR-based coverage probabilities $P_c[P_\mathcal{Y}]$ remain invariant to the change in

the cell size because the relative sum interference remains the same for a given $\bar{N}$. How noise and interference together limit the scalability of a LoRa network can be observed from the joint coverage probability $P_c[P_{\mathrm{SNR}} \cdot \mathcal{Y}]$ curves in Fig. 4(a) and (b). From these results, it can be concluded that if an EDs achieves full coverage in absence of any interference, the coverage probability under both the co-SF and inter-SF interference mainly determines the network scalability with an increasing number of EDs.

Fig. 5 shows the contour of joint coverage probability $P_c\left[P_{\mathrm{SNR}} \cdot P_{\mathrm{SIR}}^{\mathrm{II}}\right]$ for possible channel configurations of a LoRa network with respect to duty cycle and transmit power. These settings correspond to h1.4, h1.5, and h1.6 subbands of ERC recommendations [27], and can serve as a useful indicator for network dimensioning. For example, if a smart application such as smart metering, requires a certain coverage probability, which translates directly into quality of service, then for a given cell radius, the number of EDs operating on a frequency can be determined or suggested. Fig. 5(a) and (b) shows that as the duty cycle increases, the number of devices that can achieve a certain coverage probability with a given cell size decreases

TABLE IV
PARAMETERS OF SF ALLOCATION SCHEMES

Parm.	EIB	EAB	PLB
Width	$r_i = R/K$	$r_i = \ell_i - \ell_{i-1}$ $\ell_i = R\sqrt{i/6}$	$r_i = \ell_i - \ell_{i-1}$ $\ell_i = \{d : \mathrm{SNR}(d) \geq \theta_{\mathrm{SF}_i}\}$
Area	$a_i = \pi r_i^2 (2i-1)$	—	—

significantly. On the other hand, Fig. 5(c) shows that the cell radius increases at $p_t = 27$ dBm. However, due to permitted duty cycle of 10%, the impact of interference under concurrent transmissions becomes severe, which in turn reduces the maximum number of EDs drastically.

C. SF Allocation Strategies

So far, our scalability analysis assumes equal-width annuli for SFs' allocation, which we refer to as EIB scheme. To analyze how an SF allocation scheme influences the network performance, we compare EIB with two additional SF allocation strategies, namely *equal-area-based* (EAB) [28], and *path-loss-based* (PLB) [29], [30] schemes. The EAB scheme uses equal-area annuli while PLB defines annuli based on a path loss model and the SF-specific SNR thresholds. Using the path loss model, the PLB scheme calculates the SNR with respect to the distance. The distance at which SNR falls below the threshold for the lowest SF defines the outer boundary of the annulus, and the higher SF's allocation begins from that boundary and so on.

The annuli parameters for each scheme can be determined from Table IV. For PLB scheme, the path loss model is defined in Section III-B and the SF-specific thresholds θ_{SF} are given in Table III. The success and coverage probabilities obtained under these schemes are compared in Fig. 6. A common cell radius $R = 9.86$ km, determined by PLB strategy, is used that corresponds to the maximum distance at which the required SNR for the highest SF is satisfied.

The SNR-based success probability [see Fig. 6(a)] for EIB scheme is mostly higher than that for PLB and EAB schemes except at the cell boundary, where the same SF is utilized by each scheme, it becomes equal. Both PLB and EAB select a higher SF at a distance higher than EIB scheme, and this lag results into higher drop in their success probabilities. On the other hand, interesting observations can be made for SIR-based (with co-SF and inter-SF interference) success probability [see Fig. 6(b)]:
1) Compared to EIB, the higher area—implying higher number of co-SF interferers—and higher width—meaning more pronounced near-far conditions—of the first PLB and EAB annuli causes more performance loss.
2) The success probability for PLB improves for the subsequent annuli in comparison with EIB due to small-area annuli.
3) The effect of EAB scheme is unusual; it causes performance drop up to a certain distance and then the performance improves, mainly due to geometrical structure of EAB annuli. As the width of an outer annulus is less than an inner annulus, the near-far condition in each outer
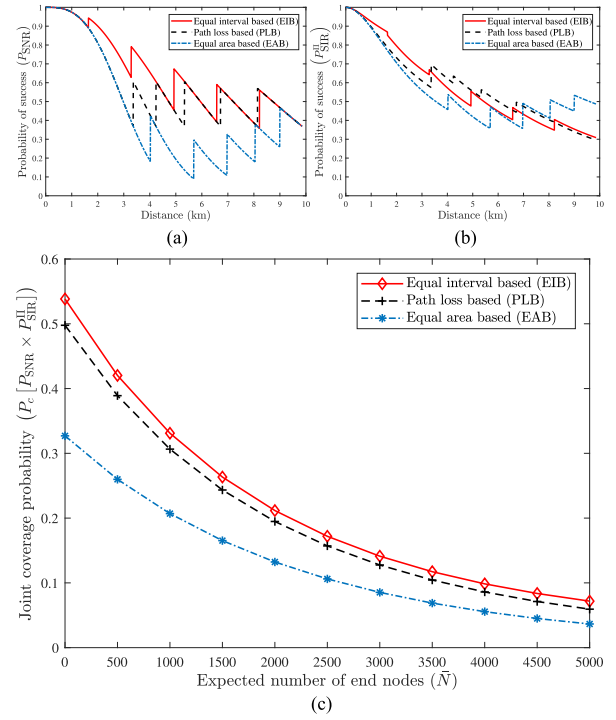

Fig. 6. Impact of SF allocation schemes on success and coverage probability at $\eta = 3$. (a) Success probability under noise. (b) Success probability under co-SF and inter-SF interference. (c) Joint coverage probability under noise and interference. Figures (a) and (b) are obtained with $\bar{N} = 1500$.

annulus is pronounced less. Therefore, after a certain annuli, the probability to achieve co-SF SIR-target at the gateway increases as compared to the previous annulus.

Fig. 6(c) reflects the mentioned drop in success probability under PLB and EAB schemes at low SF regions on the joint coverage probability. The coverage probability for EIB scheme remains higher than the other two. We also observed (not shown here) that by adding a fading margin in PLB scheme, essentially by reducing the cell size, only brings the coverage results closer for the studied SF allocation schemes.

D. Modeling a Multicell LoRa Network

In this study, interference modeling of an elemental single-cell LoRa system revealed useful scalability results. In particular, the coverage contours show how to dimension a cell with respect to its size and the number of devices, while the numbers are not that optimistic especially if the required QoS is high. However, in practical applications, the coverage demand is expected to span over a large geographical area. As a result, a LoRa network will consist of multiple cells to satisfy the coverage and QoS requisites.

In this respect, interference modeling of a multicell network is essential, which we discuss below based on our proposed approach.

In smart city applications, the devices are usually clustered with centers at the parent points, i.e., the gateways. Therefore, a clustering process must be defined for interference modeling of a

multicell network. A well-known spatial point process to model the distribution of the gateways is Poisson cluster process, where the gateways form a PPP and the devices within each cluster form an independent PPP [31]. Next, using the joint success probability under noise, intracell and intercell interference, we see how the clustering process affects the analysis.

Let $\mathcal{L}_{\mathcal{I}_{\text{intra}}}^{y_0}(\cdot)$ and $\mathcal{L}_{\mathcal{I}_{\text{inter}}}(\cdot)$ denote the LT of intracell interference from y_0—the reference cell, and intercell interference, respectively. Then, in a multicell network, the success probability of a device located at x_1 in ith annulus of y_0 is

$$P_{\text{suc}}(x_1, \delta_{ij}) = \exp\left(-\frac{\sigma\theta_{\text{SF}}}{p_t l(x_1)}\right) \times \prod_{j \in \mathcal{K}} \mathcal{L}_{\mathcal{I}_{\text{intra}}}^{y_0}\left(\frac{\delta_{ij}}{p_t l(x_1)}\right)$$
$$\times \prod_{j \in \mathcal{K}} \mathcal{L}_{\mathcal{I}_{\text{inter}}}\left(\frac{\delta_{ij}}{p_t l(x_1)}\right) \qquad (25)$$

where the first term is P_{SNR} as in (5) while the second term is P_{SIR}^{Π} given in (22) under co-SF interference (i.e., $i = j$) and inter-SF interference in a cell. Whereas, the last term considers the impact of interference from all the other cells on the success probability. At $s = \delta_{ij}/(p_t l(x_1))$, $\mathcal{L}_{\mathcal{I}_{\text{inter}}}(s)$ under the PPP distribution of the gateways Φ_G can be defined as

$$\mathcal{L}_{\mathcal{I}_{\text{inter}}}(s) = \mathbb{E}_{\Phi_G, \Phi_{m,j}, G}\left[\exp\left(-s \sum_{y_n \in \Phi_G \setminus y_0}\right.\right.$$
$$\left.\left.\times \sum_{x_{n,k} \in \Phi_{m,n,j}} p_t G_{n,k} l\left(x_{n,k} + y_n\right)\right)\right] \qquad (26)$$

where $x_{n,k} + y_n$ is the distance between the reference gateway and the device k in annulus j of cell y_n, and $G_{n,k}$ is the channel gain of the same device.

To evaluate (26) where the expectation over G remains the same [see (14)], one need to consider the distance distribution of $x_{n,k} + y_n$ and the clustering process of the "gateways" to find the expectation over $\Phi_{m,j}$ and Φ_G, respectively, which we leave as a future work.

VII. CONCLUSION

In this paper, we investigated the impact of interference on a LoRa network caused by simultaneous transmissions using the same SF as well as different SFs. While, the co-SF interference is natural and requires SIR protection to have any benefits from capture effect, the imperfect orthogonality among SFs can also cause a significant impact in high-density deployment of devices. To this end, using stochastic geometry to model the interference field, we derived the SIR distributions to capture the uplink outage and coverage performance with respect to the distance from the gateway. The SIR distributions are derived based on the aggregate co-SF and inter-SF interference power. The results obtained by comparing the aggregate co-SF interference alone to the corresponding upper bound based on dominant interferer, defy the validity of the argument—*LoRa is impervious to the cumulative interference effects* [11]—which is shown here to be dependent on the device density.

Moreover, our analysis reveals that the network scalability under the joint impact of co-SF and inter-SF interference is more accurate compared to the optimistic results usually reported when considering co-SF alone. We showed in a LoRa frequency channel only a limited number of devices can successfully transmit, otherwise the devices would waste energy in retransmissions of collided packets. In particular, for higher SFs this effect is more noticeable due to lower success probability. We summarized the usefulness of our analytical models for: first, network dimensioning under reliability constraints using contour plots for three baseline LoRa channel settings, second, interference modeling of a multicell LoRa network. In addition, we analyzed the network performance for three SF allocation schemes and showed that a simple equal-width-based scheme yields better results than the equal-area-based and path-loss-based schemes.

REFERENCES

[1] M. Centenaro, L. Vangelista, A. Zanella, and M. Zorzi, "Long-range communications in unlicensed bands: The rising stars in the IoT and smart city scenarios," *IEEE Wireless Commun.*, vol. 23, no. 5, pp. 60–67, Oct. 2016.

[2] G. A. Akpakwu, B. J. Silva, G. P. Hancke, and A. M. Abu-Mahfouz, "A survey on 5G networks for the Internet of Things: Communication technologies and challenges," *IEEE Access*, vol. 6, pp. 3619–3647, 2018.

[3] A. D. Zayas, C. A. G. Pérez, Á. M. R. Pérez, and P. Merino, "3GPP evolution on LTE connectivity for IoT," in *Integration, Interconnection, and Interoperability of IoT Systems*. New York, NY, USA: Springer, 2018, pp. 1–20.

[4] U. Raza, P. Kulkarni, and M. Sooriyabandara, "Low power wide area networks: An overview," *IEEE Commun. Surveys Tut.*, vol. 19, no. 2, pp. 855–873, Apr./Jun. 2017.

[5] F. Adelantado, X. Vilajosana, P. Tuset-Peiro, B. Martinez, J. Melia-Segui, and T. Watteyne, "Understanding the limits of LoRaWAN," *IEEE Commun. Mag.*, vol. 55, no. 9, pp. 34–40, Sep. 2017.

[6] N. Varsier and J. Schwoerer, "Capacity limits of LoRaWAN technology for smart metering applications," in *Proc. IEEE Int. Conf. Commun.*, May 2017, pp. 1–6.

[7] S. Tripathi and S. De, "An efficient data characterization and reduction scheme for smart metering infrastructure," *IEEE Trans. Ind. Informat.*, 2018, doi: 10.1109/TII.2018.2799855.

[8] D. Alahakoon and X. Yu, "Smart electricity meter data intelligence for future energy systems: A survey," *IEEE Trans. Ind. Informat.*, vol. 12, no. 1, pp. 425–436, Feb. 2016.

[9] V. C. Gungor *et al.*, "A survey on smart grid potential applications and communication requirements," *IEEE Trans. Ind. Informat.*, vol. 9, no. 1, pp. 28–42, Feb. 2013.

[10] Semtech, "LoRa modulation basics, AN1200.22," Revision 2, May 2015.

[11] O. Georgiou and U. Raza, "Low power wide area network analysis: Can LoRa scale?" *IEEE Wireless Commun. Lett.*, vol. 6, no. 2, pp. 162–165, Apr. 2017.

[12] D. Croce, M. Gucciardo, S. Mangione, G. Santaromita, and I. Tinnirello, "Impact of LoRa imperfect orthogonality: Analysis of link-level performance," *IEEE Commun. Lett.*, vol. 22, no. 4, pp. 796–799, Apr. 2018.

[13] M. C. Bor, U. Roedig, T. Voigt, and J. M. Alonso, "Do LoRa low-power wide-area networks scale?" in *Proc. 19th ACM Int. Conf. Model. Anal. Simul. Wireless Mobile Syst.*, 2016, pp. 59–67.

[14] A. Augustin, J. Yi, T. Clausen, and W. M. Townsley, "A study of LoRa: Long range & low power networks for the internet of things," *Sensors*, vol. 16, no. 9, p. 1466, 2016.

[15] F. V. den Abeele, J. Haxhibeqiri, I. Moerman, and J. Hoebeke, "Scalability analysis of large-scale LoRaWAN networks in ns-3," *IEEE Internet Things J.*, vol. 4, no. 6, pp. 2186–2198, Dec. 2017.

[16] K. Mikhaylov, J. Petaejaejaervi, and T. Haenninen, "Analysis of capacity and scalability of the LoRa low power wide area network technology," in *Proc. 22th Eur. Wireless Conf.*, May 2016, pp. 1–6.

[17] D. Bankov, E. Khorov, and A. Lyakhov, "Mathematical model of LoRaWAN channel access with capture effect," in *Proc. IEEE 28th Annu. Int. Symp. Pers., Indoor, Mobile Radio Commun.*, Oct. 2017, pp. 1–5.

[18] O. B. Seller and N. Sornin, "Low power long range transmitter," U.S. Patent 9 252 834, Feb. 2, 2016.

[19] N. Sornin and A. Yegin, "LoRaWAN 1.1 Specification," *LoRa Alliance*, Oct. 2017.

[20] C. H. Liao, G. Zhu, D. Kuwabara, M. Suzuki, and H. Morikawa, "Multi-hop LoRa networks enabled by concurrent transmission," *IEEE Access*, vol. 5, pp. 21 430–21 446, 2017.

[21] ATDI, "LoRa simulation using ATDIs RF solution." 2016. [Online]. Available: http://www.atdi.com/wp-content/uploads/2016/07/LoRa.pdf, Accessed on: Jan. 2018.

[22] M. Aljuaid and H. Yanikomeroglu, "Investigating the Gaussian convergence of the distribution of the aggregate interference power in large wireless networks," *IEEE Trans. Veh. Technol.*, vol. 59, no. 9, pp. 4418–4424, Nov. 2010.

[23] M. Haenggi and R. K. Ganti, "Interference in large wireless networks," *Found. Trends Netw.*, vol. 3, no. 2, pp. 127–248, 2009.

[24] S. Kotz and S. Nadarajah, *Extreme Value Distributions: Theory and Applications*. Singapore: World Scientific, 2000.

[25] V. K. Rohatgi and A. M. E. Saleh, *An Introduction to Probability and Statistics*. Hoboken, NJ, USA: Wiley, 2015.

[26] I. S. Gradshteyn and I. M. Ryzhik, *Table of Integrals, Series, and Products*. New York, NY, USA: Academic, 2014.

[27] ERC Recommendation 70-03, "Relating to use of short range devices," Oct. 2017.

[28] J. T. Lim and Y. Han, "Spreading factor allocation for massive connectivity in LoRa systems," *IEEE Commun. Lett.*, vol. 22, no. 4, pp. 800–803, Apr. 2018.

[29] J. Haxhibeqiri, F. Van den Abeele, I. Moerman, and J. Hoebeke, "LoRa scalability: A simulation model based on interference measurements," *Sensors*, vol. 17, no. 6, 2017, Art. no. 1193.

[30] D. Bankov, E. Khorov, and A. Lyakhov, "Mathematical model of LoRaWAN channel access," in *Proc. IEEE 18th Int. Symp. World Wireless, Mobile Multimedia Netw.*, Jun. 2017, pp. 1–3.

[31] R. K. Ganti and M. Haenggi, "Interference and outage in clustered wireless ad hoc networks," *IEEE Trans. Inf. Theory*, vol. 55, no. 9, pp. 4067–4086, Sep. 2009.

Aamir Mahmood (M'18) received the B.E. degree in electrical engineering from National University of Sciences and Technology, Islamabad, Pakistan, in 2002, the M.Sc. and D.Sc. degrees in communications engineering from Aalto University School of Electrical Engineering, Aalto, Finland, in 2008 and 2014, respectively.

He was a Research Intern with Nokia Research Center, Helsinki, Finland, in 2014, and a Visiting Researcher with Aalto University in 2015–2016. Since 2016, he is a Postdoctoral Researcher with the Department of Information Systems and Technology, Mid Sweden University, Sundsvall, Sweden. His research interests include energy-delay efficient radio resource allocation, RF interference/coexistence management, and analysis and optimization of low-power wide-area network technologies.

Emiliano Sisinni (S'02–M'04) received the M.Sc. degree in electronics engineering and the Ph.D. degree in electronic instrumentation from the University of Brescia, Brescia, Italy, in 2000 and 2004, respectively.

He is currently an Associate Professor of electronics with the Department of Information Engineering, University of Brescia. He has authored more than 100 international papers and published on international journals, books, patents, and conference proceedings. His activity is focused on numerical signal analysis, with a particular interest in digital signal processor-based instrumentation. His current research interests include smart sensors, wireless sensor networking, wired and wireless industrial communications, and smart devices.

Dr. Sisinni is a member of the IEEE-Instrumentation and Measurement Society-Technical Committee on Measurements and Networking and the IEEE Industrial Electronic Society-Technical Committee on Factory Automation, the International Electrotechnical Commission-Working Group on Industrial Networks (Wireless) and the International Electrotechnical Commission Working Group on Industrial Networks (Coexistence), and the International Electrotechnical Commission-Working Group on System Interface Between Industrial Facilities and the Smart Grid.

Lakshmikanth Guntupalli (S'13–M'17) received the B.Tech. degree in electronics and communications engineering from Jawaharlal Nehru Technological University, Hyderabad, India, in 2005, the M.E. degree in electronics and telecommunication engineering from the S. G. S. Institute of Technology and Science, Indore, India, in 2008, and the Ph.D. degree from the Department of Information and Communication Technology, University of Agder, Kristiansand, Norway.

He is currently a Postdoctoral Research Fellow with Mid Sweden University, Sundsvall, Sweden. His research interests include the areas of wireless sensor networks, wake-up radio networks, Internet-of-things, WiFi, coexistence of WiFi and LTE, 5G, and the performance evaluation of communication protocols and networks.

Raúl Rondón received the B.Sc. degree in electronic engineering with Simon Bolivar University, Caracas, Venezuela, and the M.Sc. degree in telecommunications engineering from the Polytechnic University of Turin, Turin, Italy. Since 2016, he has been working toward the Ph.D. degree at Mid Sweden University, Sundsvall, Sweden, specializing in time-critical wireless sensor networks.

His research interests include real-time communication, Internet-of-things, IWSN, and low energy technologies.

Syed Ali Hassan (S'07–M'12–SM'17) received the B.E.(Hons.) degree in electrical engineering from National University of Sciences and Technology (NUST), Islamabad, Pakistan, in 2004, the M.S. degree in electrical engineering from the University of Stuttgart, Stuttgart, Germany, in 2007, and the M.S. degree in mathematics and the Ph.D. degree in electrical engineering from the Georgia Institute of Technology, Atlanta, GA, USA, in 2011.

He is currently an Assistant Professor with the NUST School of Electrical Engineering and Computer Science, where he is also the Director of Information Processing and Transmission Research Group, which focuses on various aspects of theoretical communications. He was a Visiting Professor with Georgia Tech in Fall 2017. His research interest focuses on signal processing for communications.

Mikael Gidlund (M'98–SM'16) received the M.Sc. and Ph.D. degrees in electrical engineering from Mid Sweden University, Sundsvall, Sweden, in 2000 and 2005, respectively.

In 2005, he was a Visiting Researcher with the Department of Informatics, University of Bergen, Bergen, Norway. From 2006 to 2007, he was a Research Engineer and a Project Manager with Acreo AB, Kista, Sweden, where he was responsible for wireless broadband communication. From 2007 to 2008, he was a Senior Specialist and a Project Manager with Nera Networks AS, Bergen, where he was responsible for next-generation IP-based radio solutions. From 2008 to 2013, he was a Senior Principal Scientist and a Global Research Area Coordinator of wireless technologies with ABB Corporate Research, Västerås, Sweden, where he was responsible for technology and strategy plans, standardization, and innovation in the wireless automation area. He has pioneered the area of industrial wireless sensor network. Since 2014, he has been a Full Professor of computer engineering with Mid Sweden University. He has authored or coauthored more than 100 scientific publications in refereed journals. He holds more than 20 patents (granted and pending applications) in the area of wireless communications. His current research interests include wireless communication and networks, wireless sensor networks, access protocols, and security.

Dr. Gidlund was the recipient of the Best Paper Award at the IEEE International Conference on Industrial IT in 2014. He is currently the Vice-Chair of the IEEE IES Technical Committee on Cloud and Wireless Systems for Industrial Applications. He is an Associate Editor of the IEEE TRANSACTION ON INDUSTRIAL INFORMATICS.